Available online at www.sciencedirect.com
ScienceDirect
Journal of Power Sources 175 (2008) 699–711
JOURNAL OF POWER SOURCES
www.elsevier.com/locate/jpowsour

Microstructure changes in the catalyst layers of PEM fuel cells induced by load cycling Part I. Mechanical model

Feng Rong, Cheng Huang *, Zhong-Sheng Liu, Datong Song, Qianpu Wang

Institute for Fuel Cell Innovation, National Research Council Canada, 4250 Wesbrook Mall, Vancouver, BC, Canada V6T 1W5

Received 13 July 2007; received in revised form 1 October 2007; accepted 2 October 2007
Available online 9 October 2007

Abstract

To achieve a better understanding of the degradation phenomena of polymer electrolyte membrane fuel cells (PEMFCs), it is imperative to understand the mechanism of microstructure changes in the catalyst layer. To this end, a rate-dependent isotropic plasticity model with temperature- and humidity-dependent material properties is proposed to describe the viscoplasticity of the catalyst layer components. To understand the mechanism of such changes caused by the cycling of start-up and shutdown during the operation of a PEMFC, the material model, combined with the cohesive zone model and the contact model, is solved using the finite element method. The cohesive zone model and the frictional contact model are used to describe the evolution of interfaces between the protonic and the electronic conducting phases. Numerical simulation, based on the representation of the microstructure in the catalyst layers, shows that there is competition between crack initiations in the bulk material of the protonic phase and delamination between different phases. This competition plays an important role in microstructure changes in the catalyst layers. The reduction of connectivity between the protonic and the electronic conducting phases, which may explain the decrease of performance after certain duty cycles, could be contributed to by cracking or delamination.

Keywords: Microstructure changes; Cracks; Delamination; Mechanism of degradation; Catalyst layer

1. Introduction

The durability of polymer electrolyte membrane fuel cells (PEMFCs) is one of the most important issues in the push to successfully commercialize broad stationary and transportation energy applications. In fact, the lifetime of PEMFCs under steady operating conditions is about three to five times longer than under dynamic operating conditions [1,2]. For example, the lifetime of PEMFC stacks has reached over 10,000 h in stationary applications; by contrast, state-of-the-art PEMFC stacks can be run for only 2000 h in automotive applications [3–7]. Therefore, it is urgent to better understand why the lifetime in stationary and dynamic operating environments is so different and how to overcome it.

Recently, experimental studies have been undertaken to understand the mechanism of degradation and to characterize the aging phenomena as functions of time. Many researchers [3–6] have indeed observed microstructure changes when comparing aging membrane electrode assemblies (MEAs) with fresh ones. These changes or failures in MEAs result in a gradual reduction of ionic conductivity, an increase in total cell resistance, a reduction of active sites, a reduction of voltage, and a loss of output power [4]. As crucial parts of MEAs, catalyst layers (CLs) are examined post-mortem through transmission electron microscopy (TEM) and scanning electron microscopy (SEM). Many researchers believe that the microstructure changes in CLs can be seen as factors in fuel cell performance reduction [8,9]. According to experiment results, CLs show the following microstructure changes: cracking or delamination, loss of carbon-supported catalyst clusters, dissolution of the electrolyte (Nafion ionomer), catalyst particle migration, catalyst ripening, carbon coarsening, and so on [5,10]. These phenomena are relatively obvious, especially under dynamic operating conditions.

* Corresponding author. Tel.: +1 604 221 3050; fax: +1 604 221 3001.
E-mail address: cheng.huang@nrc-cnrc.gc.ca (C. Huang).

0378-7753/$ – see front matter.
doi:10.1016/j.jpowsour.2007.10.006

So the microstructure, especially in CLs, is arguably a critical point for improving the durability of PEMFCs and more and more researchers are focusing on elucidating the mechanism of microstructure changes in CLs and their effects on performance.

Microstructure changes in CLs may occur in several ways, such as chemical degradation of the ionic conducting parts or mechanical failure [3–5]. Although chemical degradation is a key factor in microstructure changes, it has been suggested that mechanical damage also plays an important role [11,12]. For example, debonding between the electrolyte and the carbon-catalyst agglomerate directly results in a loss of carbon-supported catalyst clusters, while the breaking of the electrolyte network contributes to the dissolution of the proton-conducting network [5]. Karlsson et al. [12,13] used a model to simulate the mechanical analysis of the MEA scale. As a result of the start-up and shutdown of the fuel cells, humidity and temperature fluctuate and influence the mechanical behaviour of different MEA components. Karlsson et al. found that critical residual stresses accumulate and lead to mechanical fatigue in the membranes after a hydrothermal cycle. However, the mechanism of microstructure changes in CLs is still unclear. Mechanical damage in the CL can appear as flaws or mud-cracks [4], delamination between the carbon-catalyst agglomerate and the electrolyte [10], or corrosion of carbon [6]. Cycled dynamic operating conditions should result in such mechanical damage or degradation, and this will greatly affect the decline in performance.

As discussed above, although many experiments show that microstructure changes occur in CLs after long, cycled operation of PEMFCs, so far there is no theoretical or numerical model to describe either the chemical or the mechanical aspects of this evolution in structure. The purpose of this work is, first, to establish a theoretical framework and a numerical model to investigate microstructure changes in CLs, and, second, to reveal the changing mechanism and to understand its effects on performance. As a first step, in this paper we focus only on the mechanical aspects of microstructure changes in CLs. The effects of such changes on CL performance and the modeling of the changes caused by chemical property variation will be discussed in subsequent papers.

In this paper, the primary methodology framework proposed is the finite element method (FEM); the cohesive zone model and the contact model are used to describe responses of bulk material, interfacial behaviours between Nafion and the carbon-catalyst agglomerate and contact phenomena between solids in CLs, respectively. The temperature-, humidity- and strain rate-dependent material models for Nafion are based on a literature review and empirical results. A simulation, based on a representation of CLs, is performed and shows that the failure of Nafion or the delamination between Nafion and the C/Pt agglomerate can be caused by hydrothermal cycles even in the absence of a chemical reaction. The mesh dependency of the present model is examined through the simulation of different mesh densities. Moreover, a parametric study is done to investigate the effects of different frequencies of start-up and shutdown of the PEMFC. A possible indication of performance decline is observed, based on the phase connection between Nafion and the C/Pt agglomerate. Finally, through a mechanical analysis, a basic understanding of the mechanism of microstructure changes in CLs is achieved.

2. Basic framework

The main focus of this paper is the mechanical mechanism of the evolution of CL microstructure. When a PEMFC is starting up or shutting down, the humidity and temperature in its CLs increases or decreases, respectively. When the cell is operating steadily, the humidity and temperature are relatively stable. The change in relative humidity (RH) or temperature (T) is illustrated in Fig. 1(a). In order to simulate microstructure changes caused by the duty cycles of fuel cells, we ignore the creep/relaxation processes occurring in part B and take into account only the relatively fast material fatigue process occurring in parts A and C. So only the start-up and shutdown processes of PEMFCs are considered, and the mechanical analysis is based on these cycles of RH and T, shown schematically in Fig. 1(b) and (c). The periods of RH and T cycles are t_{RH} and t_T, respectively. Based on this assumption, one mechanical model is proposed to investigate the effect of RH and T cycles, simulating the start-up and shutdown of the fuel cell.

2.1. Overview

There are three different phases in the CLs of a PEMFC: electrolyte (Nafion), pore, and carbon-catalyst (Pt, etc.) agglomerate. As indicated in Fig. 2, TEM is utilized to examine the microstructure of CLs [5].

The pore phase is considered void in the solid. The solid phases (Nafion and C/Pt agglomerate) are meshed in the domains for the sake of the FEM. The interfaces between any two of the three phases gradually change during the operation of the PEMFC when a cycled load is applied. Generally, debonding or delamination can occur between the Nafion and the C/Pt agglomerate phases, so the cohesive zone model (CZM) is used to mimic the evolution of the interfaces between these two solid phases, indicated by the dashed line in Fig. 2. The boundaries between pore and solid change because of the deformation of the solid. So the contact model is applied on these interfaces (indicated by the solid lines in Fig. 2).

2.2. Mechanical analysis model for bulk material

We start with the FEM; detailed procedures can be found in Ref. [14]. The material experiments already show that the mechanical properties of CLs exhibit a plastic or inelastic behaviour during PEMFC operation. This plastic behaviour of the materials has to be considered, as does their elasticity, in order to simulate the changes in microstructure. For this purpose, the inelastic response, incompressible plastic deformation, is assumed in our model and plasticity theories are used to characterize the elastoplastic response of the CL materials. The three key factors in the plasticity theory of CL materials are the yield criterion, the flow rule, and the hardening rule.

First, the von Mises yield criterion is adopted as the yield criterion of the CL materials. It states that yield occurs when the

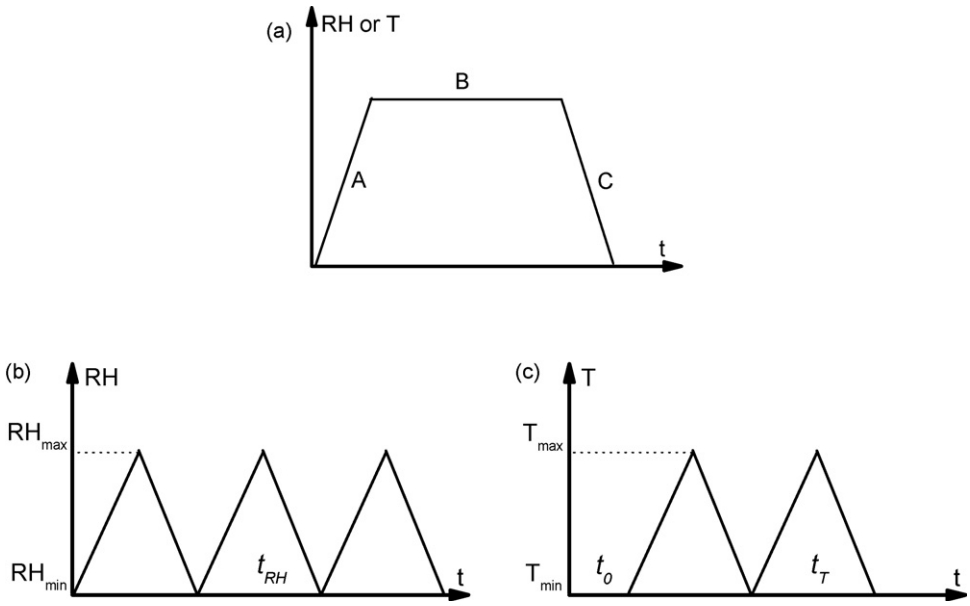

Fig. 1. (a) Schematic cycled changes of humidity (RH) and temperature (T) in CLs. Parts A and C represent the start-up and shutdown processes of fuel cells, respectively; part B represents the steady operation of fuel cells; (b) the simplified RH duty cycles, in which the period is t_{RH}; (c) the simplified T duty cycles, in which the period is t_T, and the phase difference between RH and T cycles is t_0.

von Mises yield function (J2-flow theory [15]) approaches zero. The von Mises yield function is given as

$$f(\boldsymbol{\sigma}) = \sqrt{\frac{3}{2}\mathbf{S}\mathbf{S}} - \boldsymbol{\sigma}_{\mathrm{p}}, \tag{1}$$

where $\boldsymbol{\sigma}$ is the stress tensor, $\boldsymbol{\sigma}_{\mathrm{p}}$ the yield stress of the CL materials, and $\mathbf{S}$ is the deviatoric stress. Therefore, according to the von Mises yield criterion, yield occurs when $f(\boldsymbol{\sigma}) = 0$. For $f(\boldsymbol{\sigma}) < 0$, the CL material exhibits an elastic behaviour and deforms elastically.

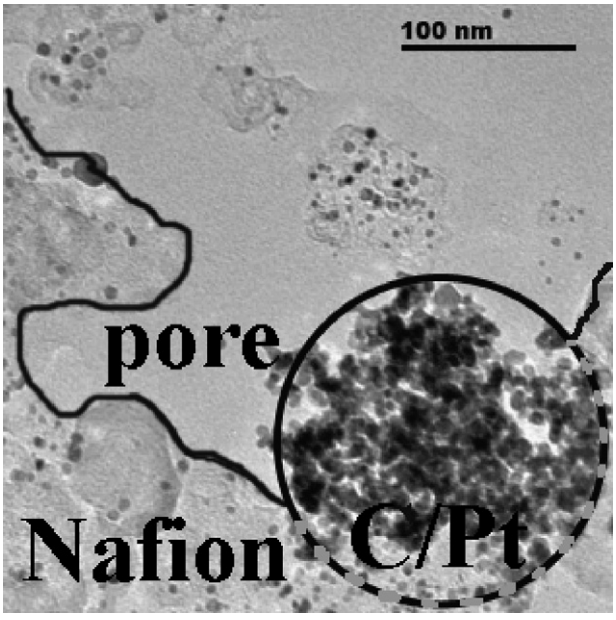

Fig. 2. TEM image of different phases in a CL, where the dashed line is the boundary between Nafion and the C/Pt agglomerate, and the solid lines are the boundaries between the pore and the other two components.

Second, the isotropic von Mises flow rule and the isotropic (work) hardening rule are used here. Flow theory predicts the direction of plastic straining increment tensor and the hardening rule describes the changing of the yield surface with progressive yielding, so that the conditions (i.e., stress states) for subsequent yielding can be established. Therefore, the plastic strain $\boldsymbol{\varepsilon}^{\mathrm{pl}}$ must be the strain that occurs in a direction normal to the yield surface and proportional to the deviatoric stress tensor,

$$\mathrm{d}\boldsymbol{\varepsilon}^{\mathrm{pl}} = \mathbf{S}\mathrm{d}\lambda, \tag{2}$$

where $\mathrm{d}\lambda$ is a scalar proportionality factor.

To introduce the effects of temperature and humidity on the behaviour of CL materials, an uncoupled theory is assumed here in which the additional temperature changes brought by the strain are ignored. So the total strain tensor can be given as follows [13]:

$$\boldsymbol{\varepsilon} = \boldsymbol{\varepsilon}^{\mathrm{e}} + \boldsymbol{\varepsilon}^{\mathrm{pl}} + \boldsymbol{\varepsilon}^{\mathrm{S}} + \boldsymbol{\varepsilon}^{\mathrm{T}}, \tag{3}$$

where $\boldsymbol{\varepsilon}^{\mathrm{e}}$ is the elastic strain, $\boldsymbol{\varepsilon}^{\mathrm{pl}}$ is the plastic strain, and $\boldsymbol{\varepsilon}^{\mathrm{S}}$and $\boldsymbol{\varepsilon}^{\mathrm{T}}$ are the strains induced by swelling and temperature, respectively. Let T_0 be a reference temperature and T the current temperature; then the thermal strains in Eq. (3) resulting from a change in temperature of an unconstrained isotropic volume are given by [13]

$$\boldsymbol{\varepsilon}^{\mathrm{T}} = \alpha I(T - T_0),$$

where α is the coefficient of thermal expansion (CTE) and I is the identity tensor. Similarly, the swelling strains caused by moisture uptake are given by [13]

$$\boldsymbol{\varepsilon}^{\mathrm{S}} = \beta I(\mathrm{RH} - \mathrm{RH}_0),$$

where RH is the relative humidity and RH_0 is the reference value for RH. β is the coefficient of moisture dependent expansion (CME) and I is the identity tensor.

So far, an isotropic plasticity model with temperature- and humidity-dependent material properties is proposed for the CL materials. However, under practical operating conditions, different frequencies of the start-up and shutdown of fuel cells will have dramatically different effects on the mechanical response of CL materials. The isotropic plasticity model discussed above does not include the effect of the strain rate, which is an indication of this frequency. Many experiments on the mechanical responses of polymer have been done to clarify its viscoplasticity. Thus the isotropic plasticity model should be modified to a rate-dependent plasticity or viscoplasticity one. The deformation of materials is assumed to develop as a function of the strain rate (or time). Many models are available to describe viscoplasticity, such as the Peirce model [16] and the Perzyna model [17]. In this paper we adopt Peirce's rate-dependent plasticity model,

$$\sigma_{\mathrm{p}} = \left[1 + \frac{\dot{\varepsilon}^{\mathrm{pl}}}{\gamma}\right]^{m} \sigma_{\mathrm{p0}}, \tag{4}$$

where σ_{p} is the material yield stress, $\dot{\varepsilon}^{\mathrm{pl}}$ the equivalent plastic strain rate, m the strain rate hardening parameter, γ the material viscosity parameter, and σ_{p0} is the static yield stress of the material, which means the yield stress under the quasi-static loading condition. Here, two parameters, m and γ, must be estimated from experimental data; this will be discussed in Section 3. The reason to choose this model over the others is the fact that, for small values of m, this model shows much better convergence. The von Mises yield function (Eq. (1)) is also rate-dependent because of viscoplasticity (Eq. (4)); that is,

$$f(\boldsymbol{\sigma}) = \sqrt{\frac{3}{2}\mathbf{SS}} - \left[1 + \frac{\dot{\varepsilon}^{\mathrm{pl}}}{\gamma}\right]^{m} \sigma_{\mathrm{p0}}.$$

In the present paper, the rate-dependent isotropic plasticity model with temperature- or humidity-dependent material properties is introduced into the FEM and solved with one of the commercial FEM software packages, such as ANSYS, NASTRAN, or ABAQUS. In this study we use ANSYS [18], in which the CZM and the contact model are already included.

2.3. Material models for interfaces in CLs

There are interfaces between the different components in CLs, such as between Nafion and the carbon/Pt agglomerate, and between pore and solid (as indicated in Fig. 2). The relationship between strain and stress on an interface is obviously different from that in bulk material. So in our simulation, the CZM, describing the behaviour of the interface between Nafion and the carbon/Pt agglomerate, and the frictional contact model, describing the behaviour of the boundaries between pore and solid, are proposed to solve this problem.

2.3.1. Cohesive zone model

Fracture or delamination along an interface between phases plays a major role in limiting the durability and the ductility of multiphase materials. In the CLs of PEMFCs, it is likely that fracture or delamination will happen along the Nafion–carbon/Pt agglomerate interface after a long period of operation under a cycled humidity or temperature load. Interfacial delamination can be modeled by traditional fracture mechanics methods such as the nodal release technique. The use of this technique requires one to select the crack path a *priori* so that double nodes (two nodes sharing the same spatial position) can be placed on it. In order to avoid this constraint, techniques are needed that directly introduce one kind of constitutive law for describing the fracture mechanism on the interfacial surface, which is taken to be a phenomenological mechanical relation between the traction and displacement jump across the surface. The CZM [19–25] adopts softening relationships between tractions and separations, which in turn introduce a critical fracture energy that is also the energy required to break apart the interface surfaces. A special set of interface elements is used to represent the interface surfaces of the materials, and the CZM is used to characterize the interface surface constitutive behaviour in ANSYS [18].

The CZM consists of a constitutive relation between the traction acting on the interface and the corresponding interfacial separation $\boldsymbol{\delta}$ (the displacement jump across the interface, which also can be described as normal separation δ_{n} and shear separation δ_{t}). An exponential form of the CZM, originally proposed by Xu and Needleman [20], uses a surface potential,

$$\Phi(\boldsymbol{\delta}) = e\sigma_{\max}\bar{\delta}_{\mathrm{n}}\left[1 - \left(1+\frac{\delta_{\mathrm{n}}}{\bar{\delta}_{\mathrm{n}}}\exp\left(-\frac{\delta_{\mathrm{n}}}{\bar{\delta}_{\mathrm{n}}}\right)\exp\left(-\frac{{\delta_t}^2}{\bar{\delta}_t^2}\right)\right)\right], \tag{5}$$

where $\Phi(\boldsymbol{\delta})$ is the surface potential, e the Euler's number (2.7182...), $\sigma_{\max}$ the maximum normal traction at the interface, δ_{n} the normal separation across the interface, δ_t the shear separation along the interface, $\bar{\delta}_{\mathrm{n}}$ the normal separation where the maximum normal traction is attained with $\delta_t = 0$, and $\bar{\delta}_t$ is the shear separation where the maximum shear traction is attained at $\delta_t = \bar{\delta}_t/\sqrt{2}$. So the traction (on both the normal direction and the shear direction) can be defined as

$$T_{\mathrm{n}} = \frac{\partial\Phi}{\partial\delta_{\mathrm{n}}} \quad \text{and} \quad T_t = \frac{\partial\Phi}{\partial\delta_t}. \tag{6}$$

From Eqs. (5) and (6), the normal traction of the interface is

$$T_{\mathrm{n}} = e\sigma_{\max}\frac{\delta_{\mathrm{n}}}{\bar{\delta}_{\mathrm{n}}}\exp\left(-\frac{\delta_{\mathrm{n}}}{\bar{\delta}_{\mathrm{n}}}\right)\exp\left(-\frac{{\delta_t}^2}{\bar{\delta}_t^2}\right), \tag{7}$$

and the shear traction is

$$T_t = 2e\sigma_{\max}\frac{\bar{\delta}_{\mathrm{n}}\delta_t}{\bar{\delta}_t^2}\left(1+\frac{\delta_{\mathrm{n}}}{\bar{\delta}_{\mathrm{n}}}\right)\exp\left(-\frac{\delta_{\mathrm{n}}}{\bar{\delta}_{\mathrm{n}}}\right)\exp\left(-\frac{{\delta_t}^2}{\bar{\delta}_t^2}\right), \tag{8}$$

Fig. 3 shows the schematic change of normal and shear tractions with normal and shear separations. Both the normal traction and the shear traction can be used to reveal the physical graph of interfacial delamination in a multiphase material.

In our simulation, the rate-dependent properties of the CZM are not explicit when compared with the bulk material. However, when the parameters in the CZM are connected to the yield stress under different loading rates, as indicated in Section 2.2 and Eq. (4), the CZM can also be considered to be a rate-dependent model.

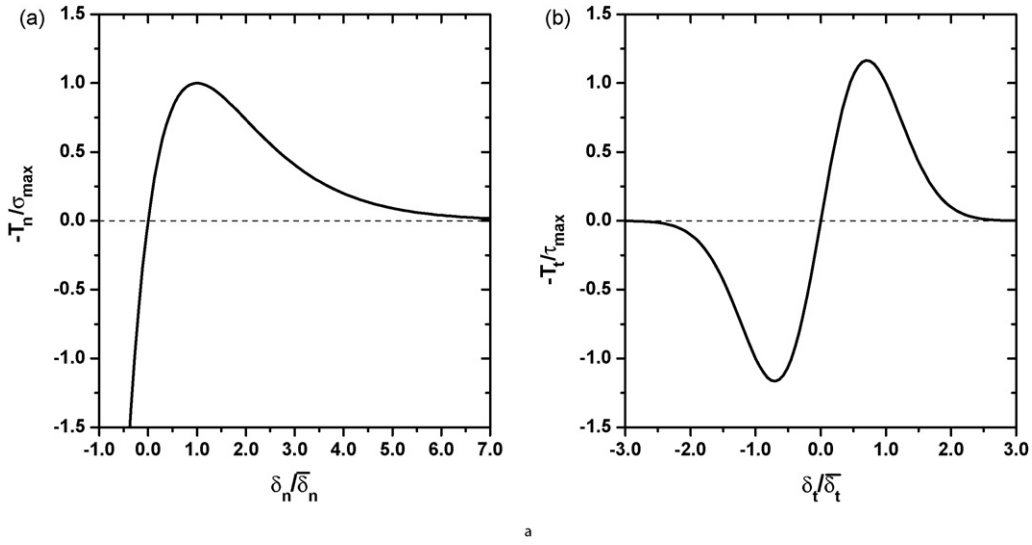

Fig. 3. Schematic of interfacial traction based on CZM: (a) normal traction and (b) shear traction.

It should be mentioned that in ANSYS [18], the constitutive relation for each cohesive surface is taken to be elastic so that any energy dissipation associated with separation is ignored. Thus the failure of the CZM elements is manually considered when the strain in the CZM exceeds one initial strain strength for the statistics of interface failure between Nafion and the C/Pt agglomerate; that is, for one CZM element, if

$$\max\left(\frac{\delta_n}{\overline{\delta_n}}, \frac{\delta_t}{\overline{\delta_t}}\right) > c_0, \tag{9}$$

it is considered to be a failure element. δ_n is the normal separation across the interface, δ_t is the shear separation along the interface, and c_0 is the coefficient corresponding to the maximum strain of interfaces. Both δ_n and δ_t are evaluated from the average values of all separations at Gauss integration points in the CZM elements.

2.3.2. Contact model

As mentioned in Section 2.3.1, the CZM is suitable only for the interface between different solid phases in CLs. Contact models must be used to describe those contact phenomena that emerge with environmental changes. Actually, contact models are highly nonlinear and require significant computer resources to solve [26]. Here, a contact model is applied on the boundary between pore and solid phases. When two solid domains, consisting of perhaps one or two kinds of materials, meet because of deformation, the contact model is applicable. On the newly formed interface, the compress force can be transferred. When there is tension occurring on this interface, the interface separates. This kind of contact phenomenon is called a non-stick contact. That is, for one contact element, if $\sigma_n > 0$, the element is considered to be separated. Here σ_n is the normal stress along the newly formed interface between two domains.

The effect of friction can be modelled through the Coulomb friction model [26], based on the transition between the sticking and sliding states. In the basic Coulomb friction model, two contacting surfaces can carry shear stresses up to a certain magnitude across their interface before they start sliding. This state is known as sticking. The Coulomb friction model defines an equivalent shear stress τ, at which sliding on the surface begins as a fraction of the contact pressure P,

$$\tau = \mu P + P_0,$$

where μ is the coefficient of friction (COF) and P_0 specifies the cohesion sliding resistance. The sticking/sliding calculations determine when transitions from sticking to sliding or vice versa occur.

In summary, the FEM, with the support of the CZM and the contact model, is proposed to calculate the mechanical response in CLs. The underlying mechanism of microstructure changes is investigated through a mechanical analysis.

3. Parameters in material models

Many researchers have done mechanical experiments on Nafion and carbon materials. In this section, some parameters used in the material models are discussed based on the experimental data in the literature.

3.1. Mechanical models of Nafion and C/Pt agglomerate materials

One of the most representative experiments was carried out by Tang and his co-workers [13]. In their experiment, a MTS Alliance RT/5 material testing system is used to test the mechanical response of Nafion 112 under different conditions by adjusting the humidity and temperature. One of their experimental results (shown in Fig. 4) gives stress–strain relations at 50% RH for different temperatures. Similar experiments have been done by other researchers on Nafion 115 [27–30], Nafion 117 [29–35], and Nafion 211 [30,36].

Based on the experimental data in the literature, a piecewise linear stress-versus-strain curve is used to describe the elastic–plastic behaviour of Nafion, as shown in Fig. 5. From the

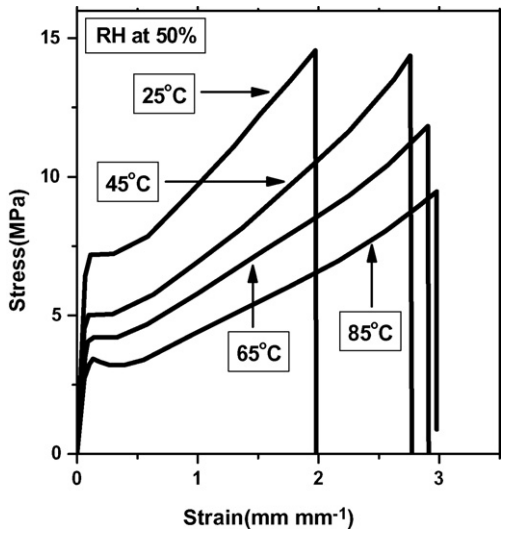

Fig. 4. Engineering stress–strain curves of tensile tests at 50% RH for different temperatures [13].

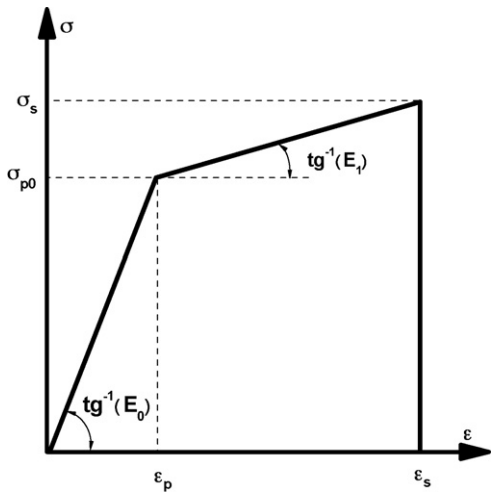

Fig. 5. The piecewise linear constitutive relationship of Nafion adopted in the model.

figure, it can be seen that six parameters are needed to describe the stress–strain relationship of Nafion: the elastic Young's modulus E_0, the plastic modulus E_1, the static yield stress σ_{p0}, the strength σ_s, the yield strain ε_p, and the break strain ε_s. When the Nafion stress σ is below its yield stress, Nafion behaves as an elastic material; when it is between its yield stress and its strength stress, Nafion behaves as a plastic material; and when it exceeds its strength stress, Nafion exhibits the characteristics of a brittle material. Among the six parameters, only four are independent, and the other two can be deducted. For simplicity, here we chose E_0, σ_{p0}, σ_s, and ε_s as the four independent parameters. The Nafion yield stress and strength stress can then

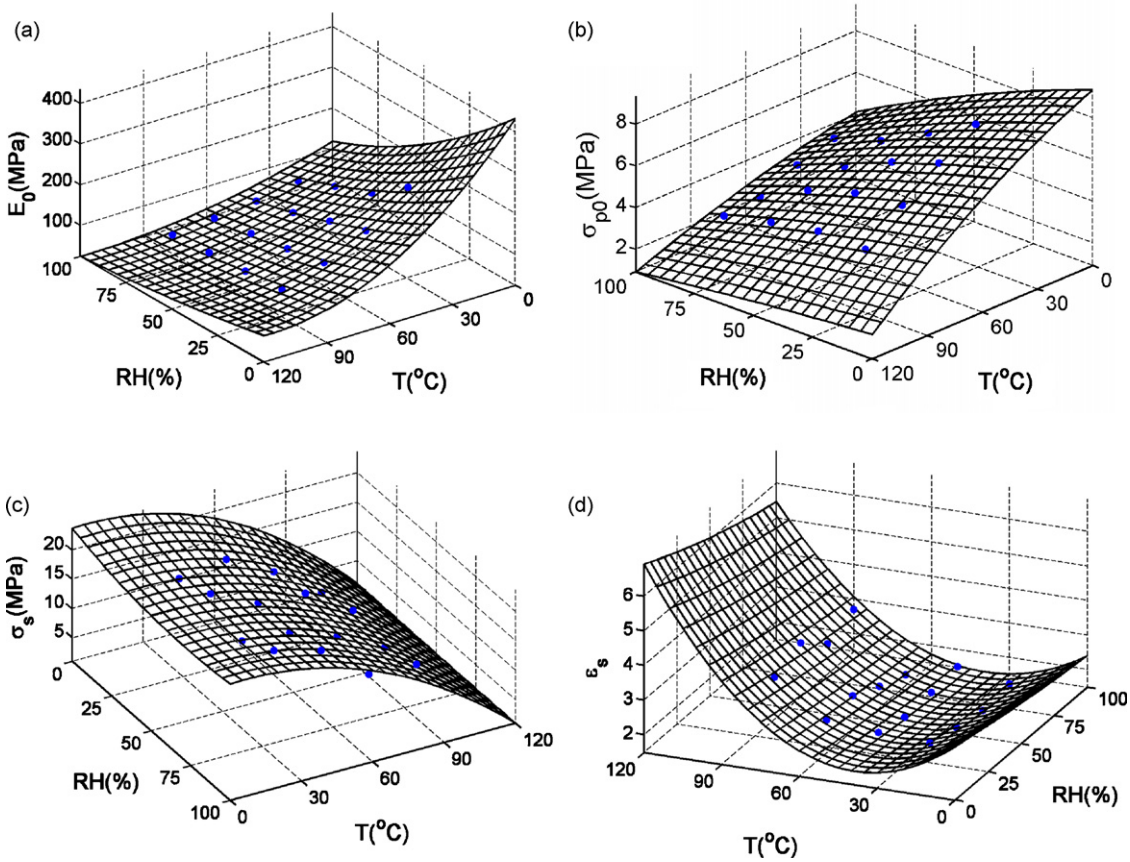

Fig. 6. Material parameters as functions of temperature and RH: (a) Young's modulus; (b) yield stress; (c) strength; (d) break strain. The points are experimental results from Refs. [13,27,30,36].

Table 1
Four independent parameters in constitutive relationship

	a_1	a_2	a_3	a_4	a_5	a_6	Error (%)
E_0	1.90E+00	−2.02E+01	5.75E+04	2.30E−02	−2.13E−01	3.87E+02	0.435
σ_{p0}	−8.27E−04	−9.60E−03	6.62E+01	−1.46E−04	−1.29E−03	7.71E+00	0.208
σ_s	1.33E−02	−6.41E−02	4.91E+02	−1.37E−03	8.00E−04	1.82E+01	0.570
ε_s	2.85E−05	−3.38E−04	3.47E+00	7.77E−04	−2.42E−03	3.07E+00	1.08

be expressed as follows:

$$\begin{cases} \sigma_{p0} = E_0 \varepsilon_p \\ \sigma_s - \sigma_{p0} = E_1(\varepsilon_s - \varepsilon_p) \end{cases}$$

The dependence of these four independent parameters on humidity and temperature is shown in Fig. 6. Many experiments have been done to study the effect of humidity and temperature on these parameters [13,27–36]. Based on the experimental data ([13,27,30,36]), the dependencies of the four independent parameters on humidity and temperature are given as

$$\frac{X}{X_r} = \left[a_1 \left(\frac{RH}{RH_r} \right)^2 + a_2 \left(\frac{RH}{RH_r} \right) + a_3 \right] \times \left[a_4 \left(\frac{T}{T_r} \right)^2 + a_5 \left(\frac{T}{T_r} \right) + a_6 \right], \quad (10)$$

where X can be E_0, σ_{p0}, σ_s and ε_s; a_i (i = 1–6) are the fitted parameters from the experimental data; RH and T are the current relative humidity and temperature, respectively; and RH_r, T_r, and X_r are corresponding reference value (here the reference values are input as the values at 30% RH and 25 °C). The fitting parameters and relative errors are given in Table 1, while Fig. 6 shows the results.

In addition, the Poisson ratio ν of Nafion can be estimated from the experimental data. Based on the work of Tang [13], ν is not sensitive to the variation of temperature and humidity and is normally taken to be a constant (ν = 0.25) [13,37]. The swelling of Nafion that occurs under different humidity levels and the expansion of Nafion at different temperatures can be characterized by the CME and CTE, respectively. Because the deviation of the CTE is relatively small compared to the deviation of the CME when RH and temperature change, the CTE is also considered to be a constant in this paper and taken as 1.23E−4/°C from Ref. [37]. The expression of the CME as a function of RH and T is adapted from Ref. [13] and [27], based on Eq. (10) and shown in Fig. 7. The fitting parameters and relative errors are given in Table 2, in which the reference value of β_r is selected as the CME at 30% RH and 25 °C.

We cannot directly obtain the rate-dependent parameters for Nafion due to the lack of experimental data. However, many experiments have been done on the viscoplasticity of PTFE. Because PTFE is the backbone of Nafion, it is reasonable to assume that the viscoplasticity of Nafion is similar to that of PTFE. Here we use the experimental data for PTFE to get the rate-dependent parameters of Nafion through Eq. (4). The experimental results for PTFE, taken from Ref. [39], are given in Fig. 8(a). The strain rate hardening parameter m and the material viscosity parameter γ can be estimated by fitting the experimental results with Eq. (4) as

$$m = 0.230 \pm 0.155; \qquad \gamma = 0.0770 \pm 0.0549,$$

In this paper, the mean values are chosen; that is, hardening parameter m is 0.230 while viscosity parameter γ is 0.0770. From Fig. 8(b), it can be seen that the ratio of the rate-dependent yield stress to the static yield stress increases from 1.0 to 1.8 when the loading strain rate changes from 0 to 1.0. The effect of such variation on the microstructure changes of CLs will be discussed in Section 4.

Based on Ref. [37], the C/Pt agglomerate is stronger than Nafion. So in this model, the C/Pt agglomerate is considered to be an elastic material and there is no failure or plasticity accumulation in it. The Young's modulus of the C/Pt agglomerate is taken to be 4.8 GPa [37].

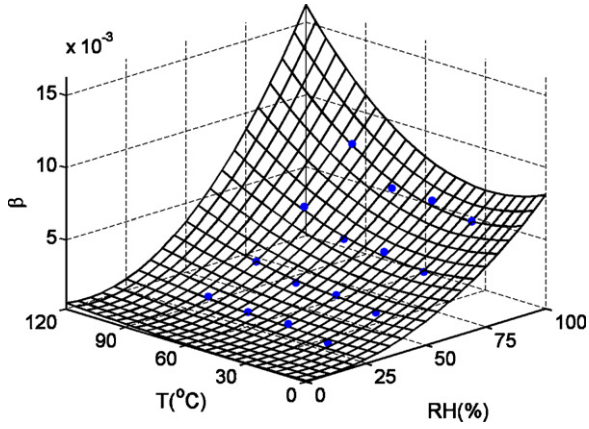

Fig. 7. CME value as a function of T and RH. The points are experimental results from Refs. [13,27].

Table 2
Parameters of humidity- and temperature-dependent CME

	β
a_1	3.35E−10
a_2	−1.81E−10
a_3	1.17E−07
a_4	4.87E−08
a_5	−1.14E−07
a_6	3.57E−04
Error (%)	0.319

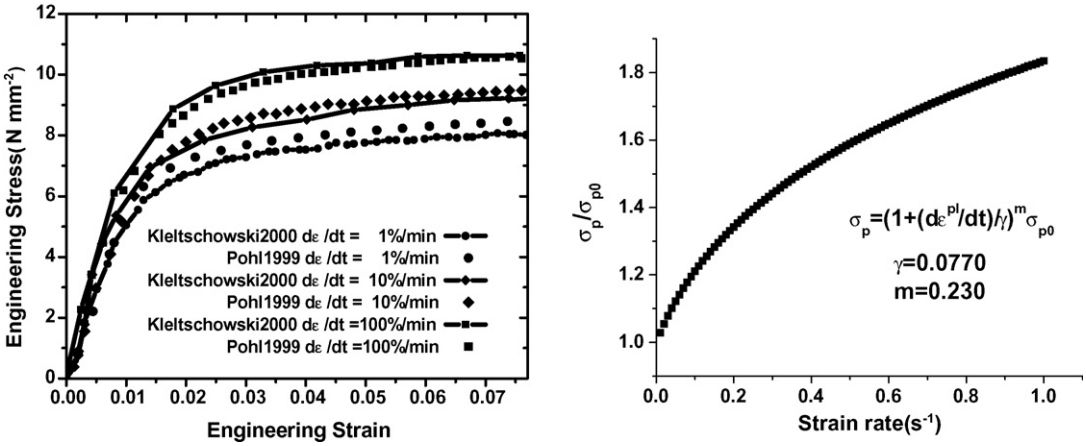

Fig. 8. (a) Strain-rate dependence of PTFE in strain-controlled tension tests using different strain rates [41]; (b) the ratio between rate-dependence yield stress and static yield stress of Nafion changes owing to strain rate.

3.2. Interfacial property of Nafion and C/Pt agglomerate

The interfacial COF μ is used for the Coulomb friction model. The COF can be found in Ref. [38] and is shown in Fig. 9. Because the loading rate is relatively small, only friction under low loading rate is considered. So μ should be 0.20 according to Fig. 9.

In order to use the CZM to simulate the boundary evolution between Nafion and the C/Pt agglomerate, three parameters in Eq. (5) need to be determined: the maximum normal traction at the interface $\sigma_{\max}$, the normal characteristic separation $\bar{\delta}_n$, and the shear characteristic separation $\bar{\delta}_t$. Empirical relationships have often been the best source for parameters in the CZM, and there are several publications on determining the parameters of the interface of the polymer (such as epoxy or PTFE) and the carbon nanotube [39]. Based on these works, $\sigma_{\max}$ is close to $E_0/10$, where E_0 is the elastic modulus of the material (in our case, Nafion). The normal characteristic separation is taken to be the same as the shear characteristic separation [20]. The maximum shear stress is close to $\sigma_p/\sqrt{3}$ [18], where σ_p is the yield stress of Nafion. The shear characteristic separation $\bar{\delta}_t$ is calculated from Eq. (8). Because of the rate-dependent characteristics of yield stress (Eq. (4)), the properties of the CZM can be also considered rate-dependent.

Eq. (9) is used to determine the failure of the CZM. Because Nafion is weaker than the C/Pt agglomerate, c_0 is assumed to be the failure strain of Nafion, which can be calculated from Eqs. (4) and (10).

It is should be mentioned that the determination of some parameters of Nafion and the C/Pt agglomerate is very difficult at this stage and we have borrowed some values for Nafion from the PTFE material in order to carry out the numerical simulation and to analyze qualitatively the mechanism of the microstructure changes in the CLs. More experimental studies or molecular simulations need to be done to characterize the material properties for Nafion and the C/Pt mixture.

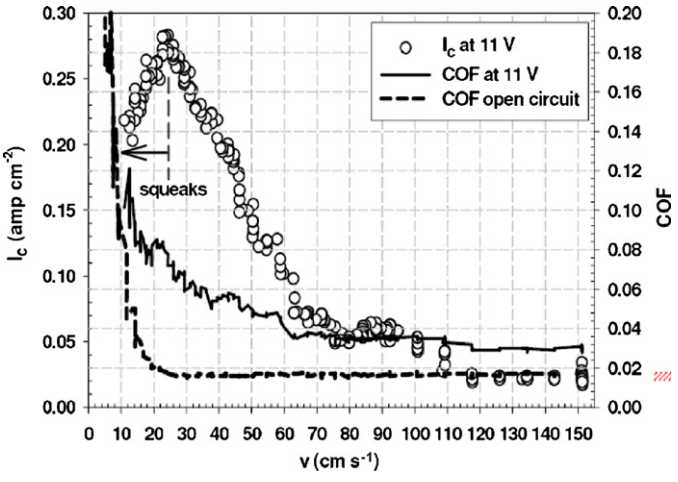

Fig. 9. COF of Nafion due to different shearing rates.

4. Numerical analysis

In this section, we simulate the microstructure changes in the CLs of a PEMFC during its operation by applying a cycled humidity and temperature load. As we pointed out in Section 1, the microstructure changes might result from chemical property variation and/or from mechanical property changes. As a first step, in this paper we focus only on the changes caused by mechanical property variation.

The aim of the simulation is to understand the basic mechanism of microstructure changes and their effects on performance based on the model proposed in Section 2. To verify the CZM and the contact model, one microstructure representation of a three-phase microstructure, including Nafion, C/Pt agglomerate and pore, is implemented. The relationship between the electrochemical performance of fuel cells and the CL microstructure is a complex one, with factors including surface area, boundary length of the three phases, and phase connectivity/tortuosity playing key roles [40]. Thus the model simulates, with the microstructure representative, the changing of phase connectivity driven by the cycled humidity and temperature.

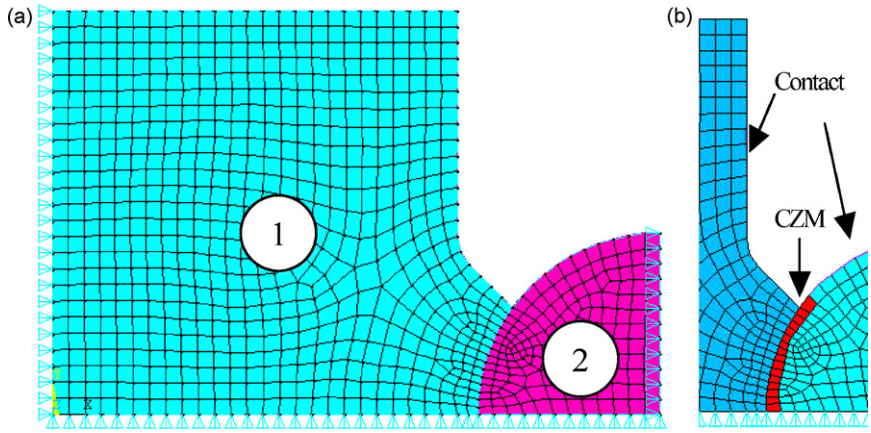

Fig. 10. (a) A typical microstructure representation of a CL, where the pink domain (domain 2) represents the C/Pt agglomerate and the cyan domain (domain 1) represents Nafion; (b) the CZM (red elements) and contact elements (purple line) in the model. (For interpretation of the references to color in this figure legend, the reader is referred to the web version of the article.)

4.1. Computational domains, boundary conditions, and cycled RH/T loads

A typical microstructure representation of CLs is illustrated in Fig. 10(a) with all three phases present. Microstructural observations [5] attest that the contact zones between the solid phases may contribute partially or completely to the voids in the whole CL. In Fig. 10(a), Nafion is represented by the cyan domain (domain 1) and has the material properties described in Section 3.1. The C/Pt agglomerate (domain 2) is the pink domain and has elastic material properties. Eight-node structural plane elements (PLANE183) are used to make up the domains of the bulk material. To simulate the interface of Nafion and the C/Pt agglomerate, the CZM is applied to the boundary elements, as indicated in Fig. 10(b). When a PEMFC is started up or shutdown, the humidity and temperature in the CLs changes periodically, and the Nafion swells or expands accordingly.

In addition, the contact model is applied, as shown in Fig. 10(b). Three-node surface-to-surface contact elements (CONTA172) are applied at the interfaces between solid and

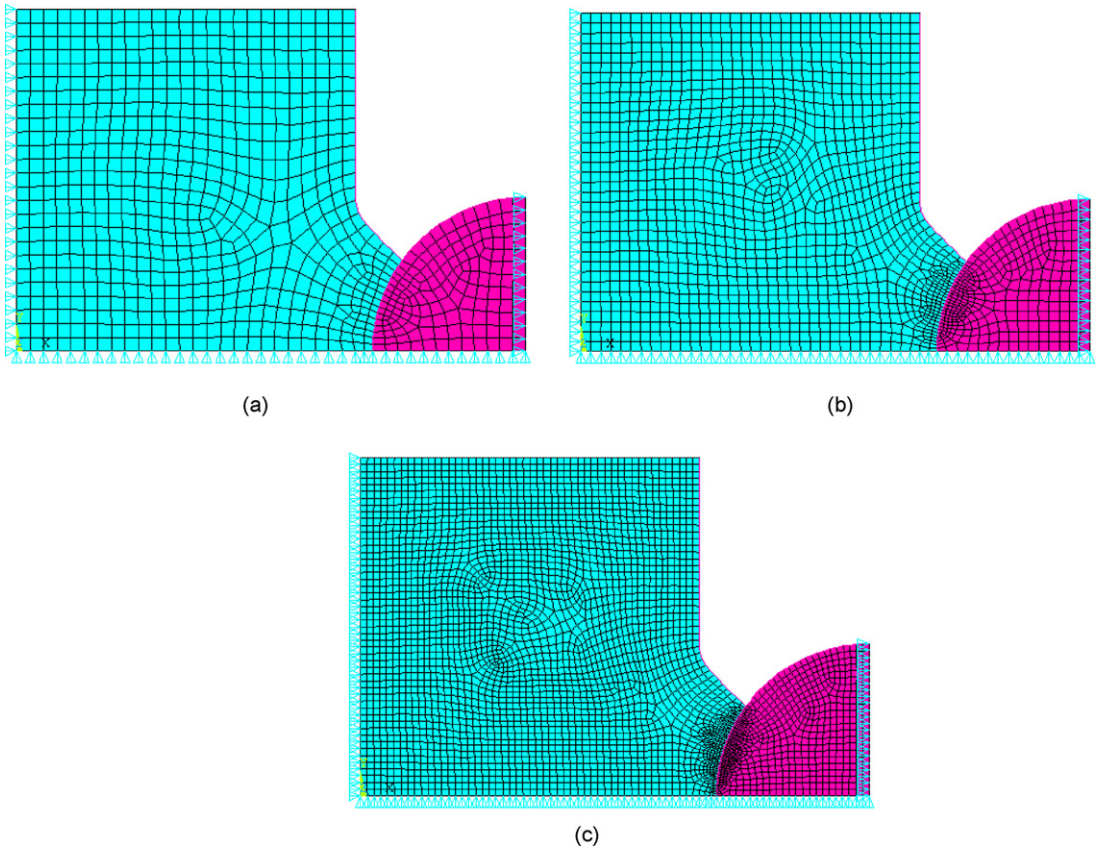

Fig. 11. Three FEM meshes with different element densities: (a) mesh 1 (865 elements); (b) mesh 2 (1739 elements); (c) mesh 3 (3824 elements).

pore, while the boundary between different solid components is meshed by six-node cohesive zone elements (INTER203). In our simulation, the plane strain condition is assumed. The symmetric boundary condition is applied on the left, right, and bottom boundaries of the whole computational domain. The symmetric boundary condition is also used on the top boundary of Nafion (domain 1), while the free boundary condition is used on the top of the C/Pt agglomerate (domain 2).

The temperature and humidity profiles come from Ref. [12]. We take the driving force for the microstructure changes in the CLs to be the cycled change of RH and T, as shown in Fig. 1. For simplicity, the periods of humidity and temperature are equal ($t_{RH} = t_T$). The relative humidity starts from $t = 0$ while the temperature begins after a 2-s delay ($t_0 = 2$ s), as shown in Fig. 1(b) and (c). The maximum and minimum values of the RH are $RH_{max} = 90\%$ and $RH_{min} = 30\%$, respectively. The maximum and minimum values of temperature are $T_{max} = 85\,^{\circ}C$ and $T_{min} = 25\,^{\circ}C$, respectively.

4.2. Mesh dependency of the model and phase connectivity evolution

The CZMs are surface elements (line elements in 2D). The kinematics of CZM allows for displacement jump discontinuities across them. And the elements incorporate a constitutive law, which relates the displacement discontinuity to the cohesive force to be transmitted across the element. Although somewhat successful in yielding numerical results that correlate sufficiently well with experimental results, this method still constrains the crack path to evolve only along the interelement boundaries of the underlying FEM grid. Therefore, the present numerical model using the CZM may require mesh sensitivity studies to verify that the underlying FEM grid is not interfering with the physics of the problem. Fig. 11 shows the three meshes, corresponding to different numbers of elements (865, 1739, and 3824, respectively), used to study the mesh dependence of the present model.

In addition, although a comprehensive analysis of the microstructure changing performance correlation is beyond the scope of this paper, the preliminary analysis below demonstrates the use of the proposed model to extract key microstructure features. Phase connectivity is the interface between Nafion and the C/Pt agglomerate and is the key factor for judging the tortuosity of protonic and electronic transport paths. Thus it is widely considered in determining effective contact area, effective chemical reaction rate, and percolation limits. From the proposed model, the connection between Nafion and the C/Pt agglomerate can be determined by simply calculating the contact length between them. The phase connectivity, that is the contact length between different solid components in CLs, can be measured after certain cycles based on the simulation, as shown in Fig. 12. In all simulations, the periods of humidity and temperature cycles are 400 s.

For all cases in the present simulations, no numerical divergence was encountered. Although there are indeed some mesh sensitivities in the present method, the same trend can be seen in all three simulations. As shown in Fig. 12, for the simulation based on mesh (a), the phase connectivity decreased 2.9% of the

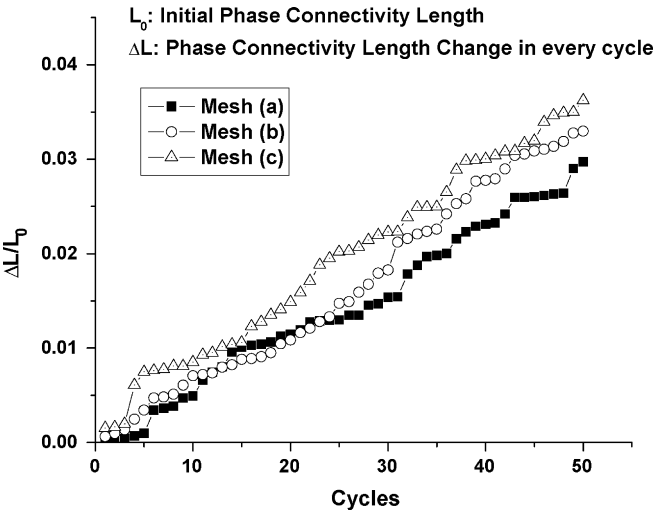

Fig. 12. Decrease of connectivity between Nafion and C/Pt agglomerate ($t_{RH} = t_T = 400$ s) based on three different mesh densities.

whole initial phase connectivity after 50 cycles. For mesh (b), the connectivity decreased 3.2%, while the connectivity decreased 3.6% for mesh (c). This shared phenomenon cannot be caused by numerical error accumulation because, based on the convergence of the FEM, denser FEM grids may converge to the true solution rather than to more errors. The physics of the problem, which is the decrease of phase connectivity after certain duty cycles, is not affected by the mesh sensitivity of the model. Therefore, the convergence and stability of the proposed model can be proven from these mesh dependency studies.

Moreover, this kind of connectivity between Nafion and the C/Pt agglomerate should be proportional to the effective electrochemical reaction surface in the CLs based on the three-phases surface model. In addition, this decrease indicates the possibility of agglomerate growth. The reduced connectivity induced by the cycled humidity and temperature change could indicate a decrease in performance.

4.3. Basic understanding of microstructure changes based on parametric study

Because there are so few mechanical experiments on Nafion and the interface between Nafion and the C/Pt agglomerate and the proposed model is hard to validate by experiment, it is necessary to study the effects of different parameters on the microstructure changes. It should be emphasized that our purpose is to analyze qualitatively the mechanism induced by the duty cycles based on the parametric study. However, this parametric study cannot be a substitute for experimental validation. On the contrary, experimental validation is urgently needed to confirm our understanding.

Based on the simulation of mesh (b), Fig. 13 shows the evolution of both the interfacial delamination fracture energy at the boundary between different components and the plastic Mises strain in Nafion. According to Fig. 13(a), when the humidity and temperature begin to increase, the Nafion swells and the delamination fracture energy in the CZM accumulates. When Eq. (9)

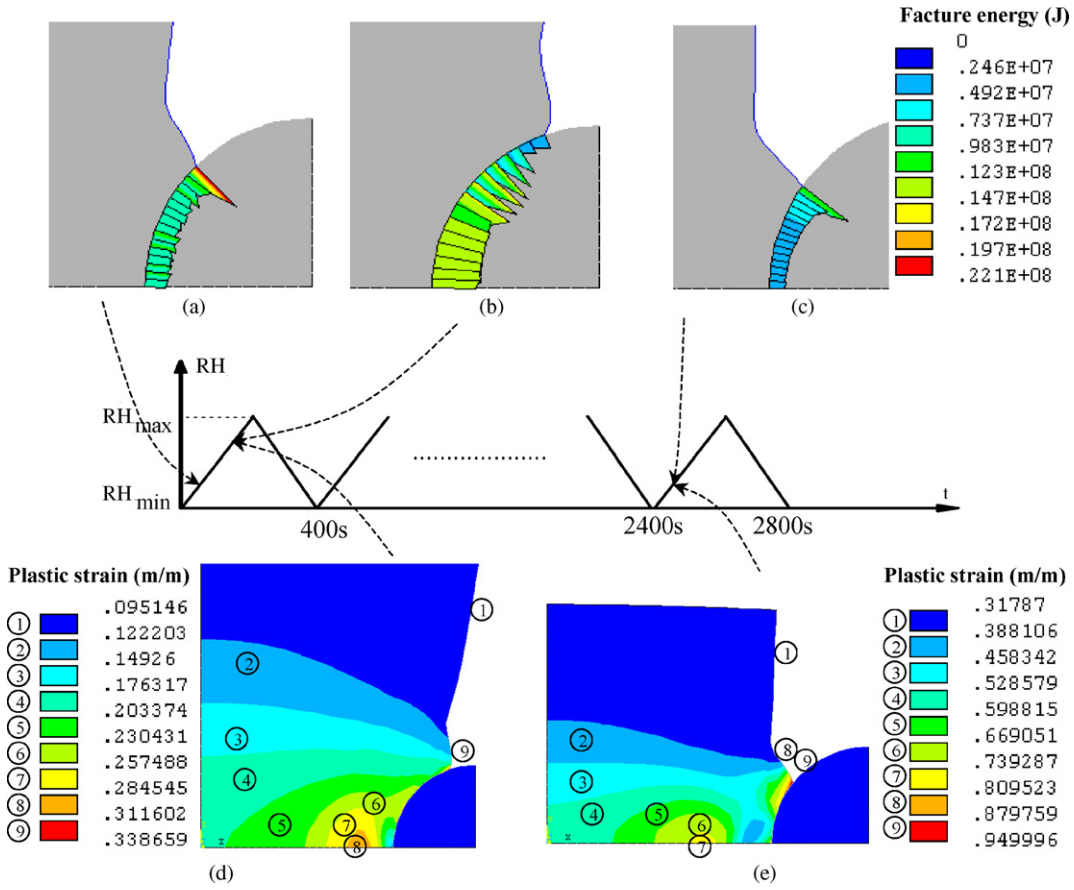

Fig. 13. (a) The delamination fracture energy pattern in CZM at 32 s; (b) the delamination fracture energy pattern in CZM at 116 s; (c) the delamination fracture energy pattern in CZM at 2432 s ((a)–(c) share the same legend); (d) the plastic Mises strain pattern in Nafion at 116 s. There is no plastic strain accumulated in Nafion at 32 s; (e) the plastic Mises strain pattern in Nafion at 2432 s. There is crack initiation in Nafion close to the top of the boundary between the different components at the next step ($t_{RH} = t_T = 400$ s).

is satisfied as the result of fracture energy accumulation in one CZM element, that element is considered to be the failure one. So as shown in Fig. 13(b), the element at the triple boundary of Nafion, C/Pt agglomerate, and pore failed at 116 s. Meanwhile, the plastic strain accumulates in the Nafion. Because the energy in the Nafion dissipates when the CZM element fails at 116 s, delamination between Nafion and the C/Pt agglomerate occurs. At the same time, the plastic energy is also accumulating in the Nafion. There is no plastic strain in the domain of the Nafion at 32 s, because it is just the beginning of the simulation. Therefore the pattern is not shown in Fig. 13. The plastic Mises strain pattern at 116 s is shown in Fig. 13(d). At 2432 s, the strain in the Nafion at the top of the interface between the different solid components exceeds its strength (as indicated in Fig. 13(e)). Thus there is crack initiation in the Nafion from that element.

Therefore, as the cycled humidity and temperature change, the plastic strain accumulates in the Nafion, resulting in fatigue (Fig. 13(d) and (e)). If there is no other mechanism for the microstructure changes, this kind of plasticity accumulation results in crack initiation and propagation in the Nafion. However, with the delamination fracture energy accumulating (in the CZM elements, Fig. 13(a, b, c)) on the interface between Nafion and the C/Pt agglomerate, there is another possible reason for microstructure changes. Thus different periods of humidity and temperature result in different accumulations of residual stress in the Nafion as well as in different energy accumulations for delamination. Crack initiation means that the strain has exceeded the break strain of the first element (whichever Nafion element or CZM element it is). For Nafion, the break strain follows Fig. 6(d) and the failure element of the CZM is determined through Eq. (9). So the competition between crack initiation and delamination plays an important role in the microstructure changes.

Because of the viscoplasticity of Nafion, the strain rate will affect the yield behaviour of the Nafion. From Fig. 8(b) it can be seen that when the hardening parameter is 0.27, the yield stress of the Nafion increases more than two times compared to the quasi-static one. So different cycle times, which also indicate the strain rate of materials, influence the microstructure changes.

In our simulations, four different periods of humidity and temperature are used, $t_{RH} = t_T = 100$ s, 200 s, 300 s, 400 s. Fig. 14 shows the initiation time of delamination between Nafion and the C/Pt agglomerate as well as the initiation time of cracking in the Nafion in these four periods. It can be seen that different periods result in different initiation times.

The shorter the cycle period of temperature and humidity is, the earlier delamination occurs. This means that if the start-up

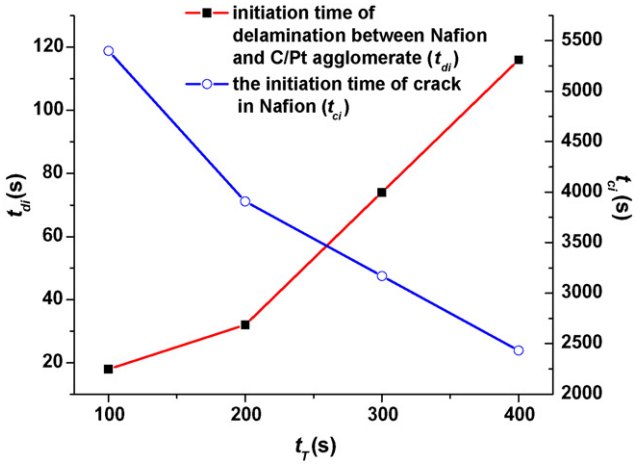

Fig. 14. The effect of different periods of humidity and temperature on the initiation time of delamination between Nafion and C/Pt agglomerate (t_{di}, denoted by the square dotted line) and on the initiation time of cracking in Nafion (t_{ci}, denoted by the circle dotted line).

or shutdown of PEMFCs is too frequent, delamination between Nafion and the C/Pt agglomerate will occur more easily. On the other hand, crack initiation in Nafion has a completely opposite tendency; that is, a shorter cycle period leads to a longer crack initiation time. This can be explained as follows. When the cycle period is shorter, the strain rate of the Nafion is greater and the corresponding yield stress is larger too. As a result, it is relatively difficult for the Nafion to yield and thus to fail. So under shorter periods of humidity and temperature, Nafion is more resistant to cracking than under longer periods. Thus there is competition between Nafion's yield-failure and Nafion–C/Pt agglomerate delamination because of the viscoplasticity of Nafion.

Simulation also shows that cracks always start from delamination between Nafion and the C/Pt agglomerate; that is, from the breakage of the CZM elements, as shown in Fig. 14. This is because, based on the material properties given in Section 3, the CZM is relatively weaker than the Nafion material under quasi-static loading.

In summary, there is competition between the delamination energy accumulation (at the interfaces between different solid components) and plastic residual strain accumulation (in the domain of the Nafion). This competition is affected by the period of temperature and humidity cycles and plays an important role in microstructure changes, resulting in either crack initiation in the Nafion or delamination between Nafion and the C/Pt agglomerate.

5. Conclusions

An FEM, with the support of the CZM and fractional contact model, is proposed to simulate the microstructure changes in CLs due to hydrothermal duty cycles of PEMFCs. Simulations are undertaken through the commercial software ANSYS by using a user subroutine. Using the humidity-, temperature-, and rate-dependent plastic material properties, the representation of the CL microstructure is simulated. Using three different mesh densities, it is found that although this method has little mesh dependency, a shared physical phenomenon can be seen in the results. Microstructure changes do occur after certain duty cycles as the result of competition between the plasticity energy accumulation in the Nafion and the delamination energy accumulation at the interface between different solid components.

Moreover, based on the parametrical study, we found that frequent start-up and shutdown of fuel cells – that is, shorter periods in RH and T cycles – lead to an earlier initiation time of delamination between the Nafion and C/Pt agglomerate, but a later initiation time of fracture in the Nafion. Finally, the length of the interface between Nafion and the C/Pt agglomerate is also investigated after certain hydrothermal cycles. It is shown that the length of the connection decreased, which may indicate performance degradation.

From the simulation results, it is found that the model itself recurs what the experiment show in its representation of microstructure in CLs. However, CL microstructure is naturally random and heterogeneous. Therefore, more practical simulations of CL microstructure will help us to understand the real problem more accurately. Work is now ongoing to construct the microstructure based on information from practical CLs and to analyze the microstructure changes due to the duty cycles of fuel cells.

Acknowledgments

The authors gratefully acknowledge the Nissan and NRC-IFCI collaboration program. FR appreciates the support of the Visiting Fellowships in Canadian Laboratories Program from the Natural Sciences and Engineering Research Council of Canada. All authors gratefully acknowledge the assistance of the referees who have provided so many valuable comments.

References

[1] S.D. Knights, K.M. Colbow, J. St-Pierre, D.P. Wilkinson, J. Power Sources 127 (2004) 127–134.
[2] D.P. Wilkinson, J. St-Pierre, in: W. Vielstich, H.A. Gasteiger, A. Lamm (Eds.), Handbook of Fuel Cells—Fundamental, Technology and Applications, John Wiley & Sons, 2003.
[3] S. Kundu, M.W. Fowler, L.C. Simon, S. Grot, J. Power Sources 157 (2) (2006) 650–656.
[4] J. Xie, I.D.L. Wood, K.L. More, P. Atanassov, R.L. Borup, J. Electrochem. Soc. 152 (5) (2005) A1011–A1020.
[5] J. Xie, D.L. Wood, D.M. Wayne, T.A. Zawodzinski, P. Atanassov, R.L. Borup, J. Electrochem. Soc. 152 (1) (2005) A104–A113.
[6] K.L. More, K.S. Reeves, J. Bentley, J. Xie, 2004, available from: http://www.hydrogen.energy.gov/pdfs/progress04/ivi2_more.pdf.
[7] N. Zamel, X. Li, J. Power Sources 155 (2006) 297–310.
[8] D. Liu, S. Case, J. Power Sources 162 (1) (2006) 521–531.
[9] J. Yu, T. Matsuura, Y. Yoshikawa, M.N. Islam, M. Hori, Electrochem. Solid-State Lett. 8 (3) (2005) A156–A158.
[10] S.-Y. Ahna, S.-J. Shinb, H.Y. Hab, S.-A. Hongb, Y.-C. Leea, T.W. Limc, I.-H. Ohb, J. Power Sources 106 (2002) 295–303.
[11] R.C. McDonald, C.K. Mittelsteadt, E.L. Thompson, Fuel Cells 4 (3) (2004) 208–213.
[12] A. Kusoglu, A.M. Karlsson, M.H. Santare, S. Cleghorn, W.B. Johnson, J. Power Sources (2006) 987–996.
[13] Y. Tang, M.H. Santare, A.M. Karlsson, S. Cleghorn, W.B. Johnson, J. Fuel Cell Sci. Technol. 3 (2006) 119–124.

[14] O.C. Zienkiewicz, R.L. Taylor, The Finite Element Method, vol. 1, 4th ed., McGraw-Hill, New York, 1988.
[15] R. Hill, The Mathematical Theory of Plasticity., Oxford University Press, New York, 1983.
[16] D. Peirce, C.F. Shih, A. Needleman, Comput. Struct. 18 (5) (1984) 875–887.
[17] P. Perzyna, Adv. Appl. Mech. 9 (1968) 313–377.
[18] ANSYS, ANSYS Documentation Release 10.0, 2006.
[19] X.P. Xu, A. Needleman, Modell. Simul. Mater. Sci. Eng. 1 (1993) 111–132.
[20] X.P. Xu, A. Needleman, J. Mech. Phys. Solids 42 (9) (1993) 1397–1434.
[21] S. Li, M.D. Thouless, A.M. Waas, J.A. Schroeder, P.D. Zavattieri, Compos. Sci. Technol. 65 (2) (2005) 281–293.
[22] S. Li, M.D. Thouless, A.M. Waas, J.A. Schroeder, P.D. Zavattieri, Compos. Sci. Technol. 65 (3–4) (2005) 537–549.
[23] M. Ortiz, A. Pandolfi, Int. J. Numer. Methods Eng. 44 (9) (1999) 1267–1282.
[24] T.I. Zohdi, P. Wriggers, Int. J. Fract. 101 (3) (2000) 9–14.
[25] M. Elices, G.V. Guinea, J. Gómez, J. Planas, Eng. Fract. Mech. 69 (2) (2002) 137–163.
[26] P. Wriggers, T.V. Van, E. Stein, Comput. Struct. 37 (1990) 319–331.
[27] M.B. Satterfield, P.W. Majsztrik, H. Ota, J.B. Benziger, A.B. Bocarsly, J. Polym. Sci. Part B: Polym. Phys. 44 (2006) 2327–2345.
[28] X. Chen, S. Hui, Polym. Test. 24 (7) (2005) 829–833.
[29] S.K. Young, K.A. Mauritz, J. Polym. Sci. Polym. Phys. 40 (19) (2002) 2237–2247.
[30] Dupont, Product Information, DuPont Nafion PFSA Membrane N-112, NE-1135, N-115, N-117, NE-1110, Perfluorosulfonic Acid Polymer, 2004.
[31] S. Kundu, L.C. Simon, M. Fowler, S. Grot, Polymer 46 (25) (2005) 11707–11715.
[32] D.R. Morris, X. Sun, J. Appl. Polym. Sci. 50 (8) (2005) 1445–1452.
[33] G. Gebel, P. Aldebert, M. Pineri, Polymer 34 (2) (1993) 333–339.
[34] Y. Kawano, Y. Wang, R.A. Palmer, S.R. Aubuchon, Polímeros 12 (2) (2002) 96–101.
[35] Y. Kawano, S.H.D. Almeida, J. Therm. Anal. Calorim. 58 (3) (1999) 569–577.
[36] K. Shi, Nafion compared with reinforced Nafion membranes, 2006, personal communication.
[37] Matweb, available from: http://www.matweb.com.
[38] S. Mazur, G.W. Foggin, C.E. Jackson, ECS National Meeting, 2006.
[39] C.D.M. Liljedahl, A.D. Crocombe, M.A. Wahab, I.A. Ashcroft, Int. J. Fract. 141 (2006) 147–161.
[40] J.R. Wilson, W. Kobsiriphat, R. Mendoza, H.-Y. Chen, J.M. Hiller, D.J. Miller, K. Thornton, P.W. Voorhees, S.B. Adler, S.A. Barnett, Nat. Mater. 5 (2006) 541–544.
[41] T. Kletschkowski, U. Schomburg, A. Bertram, Mech. Time-Depend. Mater. 8 (2) (2004) 119–135.